Annual cycles of ecological disturbance and recovery underlying the subarctic Atlantic spring plankton bloom

Michael J. Behrenfeld,[1] Scott C. Doney,[2] Ivan Lima,[2] Emmanuel S. Boss,[3] and David A. Siegel[4]

Received 27 November 2012; revised 1 April 2013; accepted 15 May 2013.

[1] Satellite measurements allow global assessments of phytoplankton concentrations and, from observed temporal changes in biomass, direct access to net biomass accumulation rates (r). For the subarctic Atlantic basin, analysis of annual cycles in r reveals that initiation of the annual blooming phase does not occur in spring after stratification surpasses a critical threshold but rather occurs in early winter when growth conditions for phytoplankton are deteriorating. This finding has been confirmed with in situ profiling float data. The objective of the current study was to test whether satellite-based annual cycles in r are reproduced by the Biogeochemical Element Cycling–Community Climate System Model and, if so, to use the additional ecosystem properties resolved by the model to better understand factors controlling phytoplankton blooms. We find that the model gives a similar early onset time for the blooming phase, that this initiation is largely due to the physical disruption of phytoplankton-grazer interactions during mixed layer deepening, and that parallel increases in phytoplankton-specific division and loss rates during spring maintain the subtle disruption in food web equilibrium that ultimately yields the spring bloom climax. The link between winter mixing and bloom dynamics is illustrated by contrasting annual plankton cycles between regions with deeper and shallower mixing. We show that maximum water column inventories of phytoplankton vary in proportion to maximum winter mixing depth, implying that future reductions in winter mixing may dampen plankton cycles in the subarctic Atlantic. We propose that ecosystem disturbance-recovery sequences are a unifying property of global ocean plankton blooms.

Citation: Behrenfeld, M. J., S. C. Doney, I. Lima, E. S. Boss, and D. A. Siegel (2013), Annual cycles of ecological disturbance and recovery underlying the subarctic Atlantic spring plankton bloom, *Global Biogeochem. Cycles*, *27*, doi:10.1002/gbc.20050.

1. Introduction

[2] High-latitude oceans experience strong seasonal variability in environmental conditions and can express large-amplitude plankton cycles with major seasonal blooms [*Longhurst*, 2007]. While representing less than one third the global area occupied by the permanently stratified tropical and subtropical biomes, these high-latitude regions support many of the Earth's productive fisheries and play a critical role in the ocean-atmosphere exchange of CO_2 [*Takahashi et al.*, 2009; *Chassot et al.*, 2010]. Potential impacts of climate warming on high-latitude marine ecosystems are thus an issue of significant ecological concern.

[3] The subarctic Atlantic is a classic example of a seasonally varying plankton ecosystem, with a late spring climax in phytoplankton concentration that is amongst the most conspicuous biological events annually recorded by global satellite ocean observations (Figure 1a). Initiation of this bloom is traditionally viewed as occurring when springtime solar radiation levels are sufficiently high and surface layer mixing depths are sufficiently shallow that phytoplankton division rates can first overcome grazing and other losses [*Sverdrup*, 1953; *Siegel et al.*, 2002]. This "bottom-up" view thus focuses on resources regulating phytoplankton-specific cell division rates, rather than factors influencing loss rates.

[4] One of the challenges in understanding bloom initiation is that historic field data in the subarctic Atlantic have been temporally biased, favoring the late spring period of maximum phytoplankton concentration. Without adequate coverage of the late autumn to early spring transition period, it is difficult to effectively evaluate the bloom initiation event, i.e., the point in time when phytoplankton-specific division rates first overcome loss rates [*Sverdrup*, 1953].

Additional supporting information may be found in the online version of this article.

[1]Department of Botany and Plant Pathology, Oregon State University, Corvallis, Oregon, USA.
[2]Department of Marine Chemistry and Geochemistry, Woods Hole Oceanographic Institution, Woods Hole, Massachusetts, USA.
[3]School of Marine Sciences, University of Maine, Orono, Maine, USA.
[4]Earth Research Institute and Department of Geography, University of California, Santa Barbara, California, USA.

Corresponding author: M. J. Behrenfeld, Department of Botany and Plant Pathology, Cordley Hall 2082, Oregon State University, Corvallis, OR 97331-2902, USA. (mjb@science.oregonstate.edu)

0886-6236/13/10.1002/gbc.20050

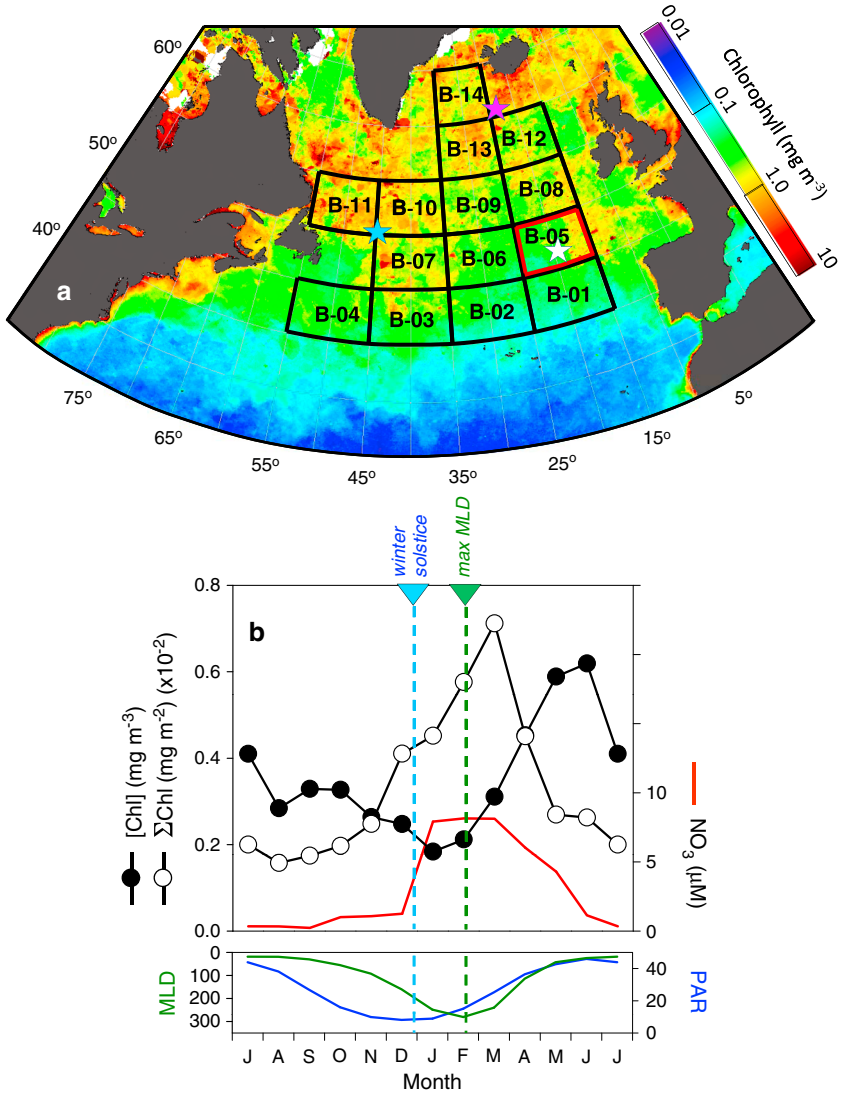

Figure 1. The subarctic Atlantic phytoplankton bloom. (a) Geographical location of the 14 regional bins. Background color shows satellite-based surface chlorophyll concentrations for June 2002, exemplifying a typical bloom. Location of JGOFS-NABE experiment (white star), location of NAB08 experiment (pink star), location of *Boss et al*. [2008] float study (blue star), and bin used to illustrate representative plankton properties in Figures 1b and 2 (red box). (b) Satellite monthly mean (1997–2007) chlorophyll concentration ([Chl]; solid circle) and depth-integrated chlorophyll inventory (ΣChl; open circle) for bin B-05. Mean monthly climatological surface nitrate (right axis; red line), surface incident PAR (mole photons m^{-2} d^{-1}; solid blue line), MLD (m; solid green line), winter solstice (dashed vertical light blue line), and month of maximum MLD (dashed green line). Note that data are plotted beginning in July on the left to focus on the autumn-through-spring period critical to bloom development.

[5] Satellite measurements continuously monitor global plankton populations, but retrieved properties are largely limited to standing stocks. However, temporal changes in stocks permit one of the only direct satellite assessments of an ecological rate: the net population accumulation rate, r (i.e., the specific rate of change in biomass). By evaluating annual cycles in satellite-observed r, *Behrenfeld* [2010] showed that mixed layer biomass first begins accumulating in the subarctic Atlantic in late autumn or early winter when growth conditions for phytoplankton are deteriorating and approaching their worst. These findings challenged traditional "bottom-up" notions of the bloom by showing that initiation occurs when phytoplankton-specific division rates (μ) are declining (rather than increasing) and that throughout the blooming period, changes in μ are not reflected by similar changes in r. It was therefore proposed that bloom dynamics reflect subtle disruptions in the balance between phytoplankton division and loss rates and that these disruptions are initiated largely by physical dilution effects during mixed layer deepening. This view was termed the "dilution-recoupling hypothesis" [*Behrenfeld*, 2010].

[6] To further test the satellite-based results, *Boss and Behrenfeld* [2010] examined 2 years of optical profiling float data from the subarctic Atlantic (blue star in Figure 1a). These in situ data confirmed the earlier finding that mixed layer biomass begins accumulating during

autumn/winter mixed layer deepening (i.e., prior to spring-time restratification) and demonstrated that satellite retrievals of net population accumulation rates are not compromised by uncertainties in phytoplankton vertical structure over the blooming phase of the annual cycle.

[7] Objectives of the current study were twofold. First, we wished to evaluate whether key features in the annual cycle of subarctic Atlantic phytoplankton observed by satellite [*Behrenfeld*, 2010] are reproduced by an established global-scale ocean ecosystem model. For this exercise, we employed the Biogeochemical Element Cycling–Community Climate System Model (BEC-CCSM) [*Doney et al*., 2009a] and divided the satellite and model data for the subarctic Atlantic basin into fourteen 5° latitude by 10° longitude bins (Figure 1a). Twelve of these bins are identical to those used in *Behrenfeld* [2010]. Our second objective, assuming the first evaluation proved successful, was to use the detailed characterization of ecosystem interactions in the BEC-CCSM to further investigate the underpinnings of the subarctic Atlantic bloom, from initiation to climax, in the context of its temporal evolution as a coupled physical-ecological system.

[8] Our analysis shows that the BEC-CCSM gives an early winter onset for the blooming phase of the annual cycle that is similar to satellite results. This initiation is strongly influenced by the physical disruption of phytoplankton-grazer interactions associated with a rapidly deepening mixed layer. We find that the extent of this disruption is proportional to the depth of winter mixing, implying that reduced winter mixing associated with climate warming may dampen high-latitude plankton cycles. During the restratification period, improvements in light conditions help prolong the bloom through the spring by allowing phytoplankton-specific division rates to slightly outpace rapidly increasing loss rates. Our results emphasize that phytoplankton blooms cannot be interpreted as a simple consequence of a single growth-regulating factor such as light but rather are expressions of slight ecosystem imbalances that are tightly coupled with variability in the physical environment.

2. Methods

[9] For this study, treatment of satellite data and binning over the subarctic Atlantic basin were nearly identical to those in *Behrenfeld* [2010], and only minor modifications were made to the BEC-CCSM. The following sections provide a brief overview of our methods and describe any changes made from previous analyses. Additional details on methods can be found in the cited publications and in the supporting information accompanying this paper.

2.1. Satellite Data Analysis

[10] Seasonal cycles in North Atlantic phytoplankton were investigated using 8 day resolution remote sensing data from the Sea-viewing Wide Field-of-view Sensor (SeaWiFS) [*McClain*, 2009]. Our analysis deviates from that of *Behrenfeld* [2010] in that (1) the satellite time series was extended to the period January 1998 to December 2007, (2) we added two North Atlantic bins (B-04 and B-11; Figure 1a) that were not included in the earlier study, and (3) the SeaWiFS data employed in the current study were from an additional 2011 reprocessing of the full SeaWiFS data set (see http://oceancolor.gsfc.nasa.gov). As in the earlier study, the 5° latitude by 10° longitude bins are defined to avoid continental margins (except bin B-11) and to minimize the influence of advection (relative to processes occurring within a bin) between 8 day periods while still capturing spatial variability in phytoplankton seasonal properties. The lowest latitude bins (B-01 to B-04) lie between 40°N and 45°N. In the northernmost bins (B-08 to B-14), satellite data are unavailable for a few weeks each year during midwinter due to high solar zenith angles. For orientation in Figure 1a, the site of the Joint Global Ocean Flux Study–North Atlantic Bloom Experiment (JGOFS-NABE) [*Ducklow and Harris*, 1993] is indicated by a white star, the North Atlantic Bloom 2008 study (NAB08) [*Mahadevan et al*., 2012] is marked by a pink star, and the profiling float study of *Boss and Behrenfeld* [2010] is shown by a blue star.

[11] Satellite products used as indices of phytoplankton abundance were surface chlorophyll concentration, [Chl] (mg m^{-3}), from the NASA standard OC4-V6 algorithm (the most familiar product to SeaWiFS users) and phytoplankton carbon concentration, [C_{phyto}] (mmol m^{-3}), calculated using the particulate backscattering coefficient at 443 nm from the Garver-Siegel-Maritorena algorithm [*Garver and Siegel*, 1997; *Maritorena et al*., 2002] and following the [C_{phyto}] algorithm of *Behrenfeld et al*. [2005] and *Westberry et al*. [2008].

[12] Depth-integrated carbon and chlorophyll inventories (i.e., ΣC_{phyto} and ΣChl), specific rates of biomass accumulation (r), and phytoplankton-specific division rates (μ) were assessed following *Behrenfeld* [2010] and *Boss and Behrenfeld* [2010]. Briefly, ΣC_{phyto} and ΣChl were calculated as the product of measured surface concentration and the greater of mixed layer depth (MLD) or euphotic depth (Z_{eu}), where Z_{eu} was calculated following *Morel and Berthon* [1989]. This assessment assumes uniform phytoplankton properties within an active mixing layer. This assumption is supported by in situ measurements during the late autumn-through-spring period when MLD exceeds Z_{eu} [*Townsend et al*., 1992; *Ward and Waniek*, 2007; *Boss et al*., 2008]. In the recent study of *Boss and Behrenfeld* [2010], 2 years of continuous profiling optical float data in the subarctic Atlantic showed that measured phytoplankton properties integrated through the mixed layer were closely approximated by the product of surface chlorophyll or carbon concentration and MLD over the autumn-through-spring period. This uniformity results from mixed layer transit times of a few days or less [*Backhaus et al*., 2003; *D'Asaro*, 2008]. In contrast to the autumn-through-spring period that is central to the current investigation of the subarctic Atlantic bloom, Z_{eu} typically exceeds MLD between roughly June and October [e.g., Figure 4 in *Behrenfeld*, 2010; Figure 3 in *Boss and Behrenfeld*, 2010]. Under these conditions, phytoplankton properties below the mixed layer, but still within the euphotic zone, can be significantly different from those within the mixed layer. This situation can lead to errors when extrapolating surface properties to depth. However, this vertical structure in phytoplankton biomass has little impact on conclusions of the current study regarding the late autumn-through-spring blooming period.

[13] As described in *Behrenfeld* [2010], understanding bloom dynamics requires an evaluation of the balance

between phytoplankton division (μ) and loss (l) rates within the mixed layer. The difference between these two rates defines r (i.e., $r = \mu - l$), where a positive value for r indicates an increasing phytoplankton population and a negative value indicates a decreasing population. When evaluating r from observed temporal changes in [Chl] or [C_{phyto}], it is important to consider whether the mixed layer is deepening or shoaling. Specifically, if light and nutrient conditions in the mixed layer allow μ to exceed l and the mixed layer depth is constant or shoaling, then phytoplankton concentration (mg m^{-3}) will increase over time. Under such conditions, the specific rate of biomass accumulation (r) can be calculated from two measures of biomass concentration (C_0, C_1) separated by a period of time ($\Delta t = t_1 - t_0$) following

$$r = \ln(C_1/C_0)/\Delta t. \quad (1)$$

[14] This scenario is similar to calculating μ for a laboratory phytoplankton culture where the volume of the culture is either held constant or decreases (for example, if samples are removed) between t_0 and t_1. Equation (1), however, does not permit an accurate assessment of r if the mixed layer is deepening. Specifically, if we assume that light and nutrient conditions allow the same excess of μ over l (i.e., the same r) but that mixed layer deepening dilutes the phytoplankton population with plankton-free water from below, then the observed change in phytoplankton concentration from t_0 to t_1 will be smaller than the previous scenario (i.e., a fixed or shrinking volume) and may even decrease if the dilution effect is strong enough. Under these conditions, retrieval of r requires accounting for the change in volume (V) within which the phytoplankton population is suspended during t_0 to t_1 (i.e., V_0 and V_1, respectively). Thus, modifying equation (1) to account for the purely physical effects of dilution gives

$$r = \ln[(C_1V_1)/(C_0V_0)/\Delta t. \quad (2)$$

[15] Application of equation (2) for the mixed layer deepening scenario is similar to calculating μ for a laboratory phytoplankton culture that is being diluted between t_0 and t_1, with the extreme case being a chemostat culture where a rapidly growing population is held at a constant concentration by equally rapid dilution. If equation (2) is also applied to a phytoplankton population in a fixed or shoaling mixed layer (the earlier scenario), then the resultant values of r would not only reflect the balance between μ and l within the mixed layer but would also include losses due to detrainment from the mixed layer (a purely physical process).

[16] In summary, r is calculated from satellite data using equation (2) when the volume of the actively growing phytoplankton population is being expanded by mixed layer deepening and the newly entrained water is relatively phytoplankton free. This condition occurs in the subarctic Atlantic in the late autumn and winter when the MLD $> Z_{eu}$. During springtime mixed layer shoaling, equation (1) is used to assess r, which allows the ecological processes regulating the dynamic balance between mixed layer μ and l to be isolated from the purely physical effects of detrainment. Finally, in the summer and early autumn period where the mixed layer is deepening but still shallower than Z_{eu}, the newly entrained water from depth is not plankton free. If the phytoplankton concentration in the entrained deep water is equal to that in the mixed layer, then equation (1) can be used to assess r. As the actual phytoplankton concentration below the mixed layer is not known, this approach imparts an uncertainty in retrieved r, but this uncertainty has no impact on our conclusions regarding the winter-spring bloom in the subarctic Atlantic. In summary, r was calculated from the 8 day resolution SeaWiFS data for each North Atlantic bin following

$$r = \ln\left(\sum C_{phyto\text{-}1}/\sum C_{phyto\text{-}0}\right)/\Delta t, \text{ if MLD is deepening and } > Z_{eu}, \quad (3)$$

$$r = \ln\left([C_{phyto\text{-}1}]/[C_{phyto\text{-}0}]\right)/\Delta t, \text{ if MLD is shoaling or } < Z_{eu}, \quad (4)$$

where [$C_{phyto\text{-}0}$] and $\Sigma C_{phyto\text{-}0}$ are phytoplankton carbon concentration and inventory, respectively, at t_0; [$C_{phyto\text{-}1}$] and $\Sigma C_{phyto\text{-}1}$ are phytoplankton carbon concentration and inventory, respectively, at t_1, $\Delta t = t_1 - t_0 = 8$ days; and r is the average specific rate of biomass accumulation between time points t_0 and t_1. This approach is identical to that used in *Behrenfeld* [2010] and *Boss and Behrenfeld* [2010].

[17] Phytoplankton-specific division rates (μ) were calculated as water column-integrated daily net primary production (NPP) divided by ΣC_{phyto}. NPP was calculated from the SeaWiFS data at 8 day resolution using the Vertically Generalized Production Model [*Behrenfeld and Falkowski*, 1997], where the maximum daily chlorophyll-specific light-saturated photosynthetic rate (P^b_{opt}) was described as an exponential function of sea surface temperature (SST) [*Morel*, 1991; *Campbell et al*., 2002; *Carr et al*., 2006; *Behrenfeld*, 2010].

[18] Our analysis also employed data on incident surface photosynthetically active radiation (PAR), sea surface temperature (SST), and mixed layer depth (MLD). PAR data are SeaWiFS cloudiness-corrected values. SST data are from the Moderate-Resolution Imaging Spectrometer and the Advanced Very High Resolution Radiometer (http://web.science.oregonstate.edu/ocean.productivity). PAR and SST data are from the NASA Ocean Color website (oceancolor.gsfc.nasa.gov/). MLD values were from the Fleet Numerical Meteorology and Oceanography Center (FNMOC) model [*Clancy and Sadler*, 1992] and the Simple Ocean Data Assimilation (SODA) model, where MLD was defined as the first depth where density is 0.125 kg m^{-3} greater than the surface value. This MLD criterion does not account for short-term periods of low turbulence during the spring stratification period, but these transient events are not critical to bloom development [*Mahadevan et al*., 2012] nor during convective deepening of the mixed layer in the late autumn, early winter period of bloom initiation. The merged FNMOC and SODA data sets are described in detail and downloadable at www.science.oregonstate.edu/ocean.productivity. These MLD data are based on model estimates tuned to available in situ data (i.e., they are "data-assimilating models"). As described below (see section 2.2), the BEC-CCSM also generates MLD estimates, but in this case, the data are not tuned to in situ measurements. Nevertheless, spatial and temporal variations in

MLD are similar to those from the data assimilating FNMOC and SODA estimates. All satellite-based properties requiring MLD estimates used FNMOC and SODA data, while all BEC-CCSM properties requiring MLD estimates used MLD data from the model. In section 3, MLD estimates from the data assimilating models are shown in Figures 1b, 3b, and 5a, while MLD data from the BEC-CCSM are shown in Figures 3b, 4a, and 5b.

2.2. The Hindcast Global Ocean Ecosystem-Biogeochemistry Simulation

2.2.1. Ecosystem-Biogeochemistry Module

[19] The Biogeochemical Element Cycling–Community Climate System Model (BEC-CCSM) [*Doney et al*., 2009a] is cast as a set of three-dimensional, time-varying advection diffusion equations for a suite of tracers, C:

$$\frac{\partial C}{\partial t} + \nabla \bullet \left(\vec{v}\, C\right) - \nabla \bullet (K \nabla C) = \mathrm{RHS}^{C}_{\mathrm{bio}} \tag{5}$$

[20] The physical transport is partitioned into resolved advection and parameterized eddy-mixing terms. All of the ecological-biogeochemical source/sink terms and surface and sediment fluxes are grouped into the right-hand side term, $\mathrm{RHS}_{\mathrm{bio}}$. The marine ecosystem module incorporates multinutrient limitation (N, P, Si, and Fe) on phytoplankton division and specific phytoplankton functional groups [*Moore et al*., 2002, 2004]. Model equations and parameters are provided in Table S1 in the supporting information.

[21] There are 14 main model compartments: small pico/nanoplankton, diatoms, diazotrophs, zooplankton, suspended and sinking particulate detritus, and dissolved nitrate, ammonia, phosphorus, iron, silicate, oxygen, dissolved inorganic carbon, and alkalinity. The pico/nanoplankton size class is designed to replicate the rapid and highly efficient nutrient recycling found in many subtropical, oligotrophic (low nutrient) environments. Diatoms model a larger, bloom-forming size class. Phytoplankton division rates are determined by available light and nutrients using a modified form of the *Geider et al*. [1998] dynamic growth model. Photoacclimation is parameterized with dynamically adaptive Chl:C ratios. The diazotrophs fix all required nitrogen from N_2 gas. Calcification is parameterized as a fraction of the pico/nanoplankton production and described as a function of temperature and nutrients adapted for coccolithophores. Size-structure effects are included by varying key zooplankton (e.g., partitioning of fecal pellets between suspended and sinking detritus), depending on the food source [*Lima and Doney*, 2004]. Many of the biotic and detrital compartments contain multiple elemental pools, in addition to carbon, to track flows through the ecosystem. The model has one adaptive zooplankton class that grazes on phytoplankton and large detritus.

[22] The biogeochemistry module [*Doney et al*., 2009b] is based on an expanded version of the Ocean Carbon Model Intercomparison Project biotic model [*Najjar et al*., 2007]. The module includes full carbonate system thermodynamics and air-sea CO_2 and O_2 fluxes. Gas transfer velocities are computed from the 6-hourly National Centers for Environmental Prediction winds (http://www.cdc.noaa.gov/cdc/reanalysis/reanalysis.shtml) using the quadratic wind speed relationship of *Wanninkhof* [1992]. A dynamic iron cycle is incorporated with atmospheric dust deposition, water column scavenging, and a continental sediment source (*Moore et al*. [2006a]; see also *Moore and Braucher* [2008] for a discussion on refinements of continental sediment source). Denitrification is simulated in oxygen-minimum zones following *Moore and Doney* [2007], and subsurface particle remineralization is parameterized by incorporating the mineral ballast arguments of *Armstrong et al*. [2002]. Our 3-D implementation of the ecosystem model equations and parameters follows those of *Moore et al*. [2004] with the following modifications: (1) incorporation of water column denitrification [*Moore et al*., 2006a], (2) adjustments in iron dynamics and scavenging parameters [*Moore et al*., 2006a; *Moore and Braucher*, 2008], and (3) inclusion of a temperature dependence for the phytoplankton linear mortality coefficient following a Q10 functional form [*Eppley*, 1972]:

$$\gamma(T) = \gamma(T_{\mathrm{ref}}) 2.0^{0.1(T - T_{\mathrm{ref}})}. \tag{6}$$

[23] The same form and parameter value is used for the temperature dependence of modeled phytoplankton and zooplankton growth and zooplankton mortality. The phytoplankton mortality temperature dependence was added to improve the simulated phytoplankton seasonal cycle compared to the results reported in *Doney et al*. [2009b].

2.2.2. Atmospheric Forcing and Ocean Physical Hindcasts

[24] The Parallel Ocean Program (POP) is a z-level, hydrostatic, primitive equation model integrated here with a resolution of 3.6° in longitude, 0.8° to 1.8° in latitude, and 25 vertical levels (Community Climate System Model version 3 low-resolution ocean model; *Yeager et al*. [2006]). Effects of mesoscale eddy transport are parameterized according to *Gent and McWilliams* [1990]. The *Large et al*. [1994] K-Profile Parameterization is implemented in the vertical to capture surface boundary layer dynamics and interior diapycnal mixing. The historical simulation (1958–2006) is integrated with air-sea heat, freshwater, and momentum fluxes derived from a bulk flux forcing method using atmospheric forcing data from Coordinated Ocean-Ice Reference Experiments, Corrected Interannual Forcing Version 2 available from http://data1.gfdl.noaa.gov/nomads/forms/mom4/COREv2.html [*Large and Yeager*, 2009]. *Doney et al*. [2007] presented a quantitative skill assessment of the ocean physical solutions in terms of interannual variability of temperature, sea surface height, and circulation. Mineral aerosol deposition to the ocean is simulated using a 3-D atmospheric chemical transport model [*Luo et al*., 2003; *Mahowald et al*. 2003] based on the National Centers for Environmental Prediction/National Center for Atmospheric Research reanalysis [*Kistler et al*., 2001].

[25] Initial conditions for the 3-D ocean nutrient and inorganic carbon variables are prescribed from data-based climatologies [e.g., *Key et al*., 2004]. The ecological-biogeochemical simulation is spun up for several hundred years, prior to initiating the interannual varying forcing, using a repeat annual cycle of physical forcing and dust deposition. The model ecosystem components converge to a repeat annual cycle within a few years of spin-up. The full interannual

variability in physics is initiated in a model year equivalent to calendar year 1958 and then integrated forward through 2006.

[26] Projections of future changes in ocean mixed layer depth for the 21st century are derived from the Community Climate System Model version 4 (CCSM4), a fully coupled global climate model consisting of land, atmosphere, ocean, and sea ice components [*Gent et al*., 2011]. State information and fluxes are exchanged between components daily via a coupler. The full system conserves mass and energy. The ocean component of CCSM4 is the Parallel Ocean Program version 2 (POP2), a *z*-level, hydrostatic, primitive equation model integrated with a nominal horizontal resolution of $1^\circ \times 1^\circ$ and 60 vertical levels with grid spacing of 10 m in the upper 160 m increasing to 250 m at depth [*Danabasoglu et al*., 2012]. Mesoscale eddy transport is parameterized according to *Gent and McWilliams* [1990] (GM), with a depth and time-varying GM coefficient. Interior diapycnal mixing and boundary layer dynamics are represented using the K-Profile Parameterization of *Large et al*. [1994]. The 21st century CCSM4 simulations are integrated following the protocol from the Climate Model Intercomparison Project CMIP5 [http://cmip-pcmdi.llnl.gov/cmip5/experiment_design.html], with prescribed atmospheric CO_2 from a high-emissions scenario (RCP8.5). RCP stands for Representative Concentration Pathways, which are based on specified global radiative forcing levels (in this case, +8.5 W/m^2 by 2100). Socioeconomic and emissions scenarios have been constructed to match each RCP [*Moss et al*., 2010].

3. Results

3.1. Annual Phytoplankton Cycles in the Subarctic Atlantic

[27] The most dramatic attribute of a bloom is the high abundance of phytoplankton occurring at the final stage of the event, which is often quantified by the surface chlorophyll concentration (e.g., Figure 1a). These climax concentrations, however, are a consequence of phytoplankton accumulation over a prolonged "blooming phase." Here we define the blooming phase of the annual cycle as the entire period of accumulating mixed layer phytoplankton biomass (i.e., positive values of *r*) leading up to the spring bloom climax. Key features of the blooming phase include (1) the timing of and environmental conditions at initiation (when *r* first becomes positive), (2) changes in vertically integrated chlorophyll inventories (ΣChl; mg m^{-2}) and surface chlorophyll concentrations ([Chl]; mg m^{-3}), and (3) the relationship between *r* and μ over the duration of the blooming period.

[28] As an illustration of basic patterns in phytoplankton stocks for the subarctic Atlantic, Figure 1b shows the annual cycle in satellite-derived [Chl] (solid black symbols) from the bin encompassing the JGOFS-NABE site (i.e., B-05; Figure 1a). Surface [Chl] is lowest between roughly December and February when incident photosynthetically active radiation (PAR) is minimal and the mixed layer depth (MLD) is deepest (blue and green lines, respectively, in Figure 1b, bottom). Values of [Chl] increase through spring to a maximum around June. The subsequent demise of the bloom may coincide with depletion of surface nitrate (Figure 1b, red line), silicate [*Mahadevan et al*., 2012], or iron [*Moore et al*., 2006b; *Blain et al*., 2004; *Nielsdottir et al*., 2009] or may result from overgrazing [*Banse*, 1992, 2002] or viral infection [*Suttle et al*., 1990; *Bratbak et al*., 1993; *Baudoux et al*., 2006; *Vardi et al*., 2009; *Bidle and Vardi*, 2011].

[29] The annual cycle of ΣChl (Figure 1b, open symbols) differs substantially from that of [Chl] and begins increasing in late autumn when incident light is approaching its annual minimum and the MLD is still deepening (Figure 1b, bottom). ΣChl is maximum prior to significant nutrient drawdown and then reaches a minimum during the low-nutrient, stratified summer months (Figure 1b).

[30] Annual cycles in [Chl] and ΣChl similar to those shown in Figure 1b are found for all 14 subarctic Atlantic bins (Figure S1 in the supporting information). The same basic patterns are also observed in annual cycles of satellite-based phytoplankton carbon concentration ([C_{phyto}]; mmol m^{-3}) and carbon inventories (ΣC_{phyto}; mmol m^{-2}) (Figure S2 in the supporting information). Within a given bin, strong correlations are found for the 10 year satellite time series between [Chl] and [C_{phyto}] (e.g., Figure S3a in the supporting information) and between ΣChl and ΣC_{phyto} (e.g., Figure S3b in the supporting information). Equivalent correlations were shown in Figure 1b of *Behrenfeld* [2010], along with an evaluation of intrabin variability at 8 day resolution.

3.2. Subtle Food Web Disequilibria Underlie Blooms

[31] The specific rate of change in biomass (*r*) is defined by the difference between specific division and loss rates (i.e., $r = \mu - l$). In some regions of the tropical and subtropical oceans, μ and *l* are perpetually balanced and phytoplankton abundance remains stable throughout the year (i.e., $r \approx 0$ day^{-1}) [*Behrenfeld et al*., 2005]. It has long been recognized that imbalances between μ and *l* at higher latitudes can cause phytoplankton abundances to accumulate and decrease in large-amplitude annual cycles [e.g., *Riley et al*., 1949; *Sverdrup*, 1953; *Evans and Parslow*, 1985; *Frost*, 1987; *Banse*, 1992, 2002; *Longhurst*, 2007], but few studies have evaluated complete annual cycles in μ, *l*, and *r*. Both satellite data and BEC-CCSM output allow inspection of temporal variability in these three key rate terms for the subarctic Atlantic.

[32] For the BEC-CCSM, μ is calculated from modeled light, nutrient, and temperature fields and *l* is separated into losses due to zooplankton grazing ($l_{grazing}$) and nongrazing mortality (e.g., senescence, viral lysis, and aggregate sinking) rates (section 2.2 and Table S1 in the supporting information) [*Doney et al*., 2009a]. For SeaWiFS data, *r* is calculated from observed changes in [C_{phyto}] and ΣC_{phyto} (section 2.1) [*Behrenfeld*, 2010; *Boss and Behrenfeld*, 2010]. Satellite data also allow calculation of μ as the biomass-specific net primary production rate (section 2.1) [*Behrenfeld*, 2010], which subsequently allows *l* to be estimated as $\mu - r$.

[33] Again using bin B-05 for illustration, comparison of satellite- and model-based data reveals that these two independent approaches yield nearly identical values for μ during the nutrient-enriched autumn-to-spring period that is critical to bloom development (Figure 2 a). During this time, μ decreases until the maximum mixed layer depth (MLD) is reached in February (Figure 2a, dashed green line) and then increases rapidly with subsequent mixed layer shoaling and continued increases in PAR. During summer and early autumn, the BEC-CCSM gives μ estimates that are notably

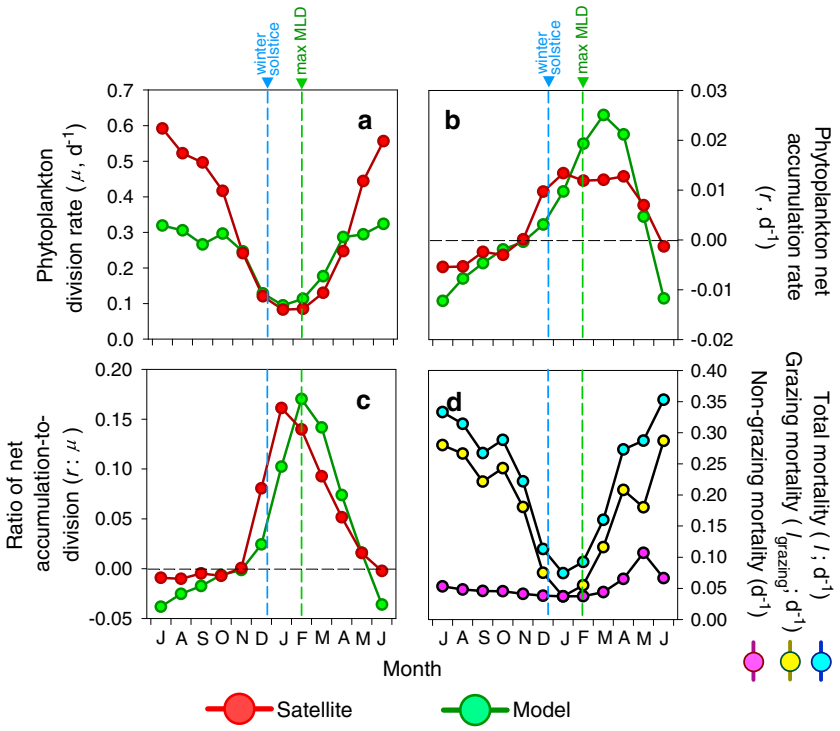

Figure 2. Satellite- (red) and model-based (green) annual cycles in key plankton properties of the subarctic Atlantic. (a) Phytoplankton-specific division rate (μ). (b) Specific rate of accumulation in phytoplankton biomass (r). (c) Ratio of net accumulation rate to division rate (r:μ). (d) BEC-CCSM-based phytoplankton mortality rates. Total mortality (l; blue), grazing mortality ($l_{grazing}$; yellow), and nongrazing mortality (pink). Data in all plots are monthly mean values for bin B-05 over the period 1997–2007. Dashed vertical light blue and green lines are as in Figure 1b. Data are plotted beginning in July on the left to focus on the autumn-through-spring period critical to bloom development.

lower than the satellite values, in part reflecting the challenge of characterizing biomass recycling during this low-nutrient period of the year. However, this summer-through-early autumn discrepancy between satellite- and model-based estimates of μ has no impact on our conclusions regarding primary processes influencing the annual blooming phase.

[34] Comparison of satellite- and model-based annual cycles in r reveals two particularly notable features (Figure 2b). First, the satellite-detected initiation of the blooming phase prior to winter solstice (when r first becomes positive) is reproduced by the BEC-CCSM. In both cases, this initiation occurs while μ is still decreasing. Second, values of r may be at or near maximal in February (low light, deepest MLD) and then show little response to the large springtime increases in μ (e.g., compare Figures 2a and 2b). This early bloom initiation has also been observed in the field near the location of bin B-05 [*Mémery et al*., 2005] In neither annual cycle of r is there any indication that mixed layer stratification in spring must surpass a critical threshold before μ can exceed l [*Sverdrup*, 1953].

[35] Values of r are one to several orders of magnitude smaller than μ (Figures 2a and 2b). Thus, the seasonal cycle in phytoplankton losses, l, must be nearly identical to the seasonal cycle in μ, implying that the annual bloom results from only subtle disequilibria between two much larger and opposing rates [*Evans and Parslow*, 1985; *Banse*, 1992; *Longhurst*, 2007; *Behrenfeld*, 2010]. In other words, the bloom is a consequence of a residual difference. This imbalance can be examined through changes in the r:μ ratio, which reflects the fraction of phytoplankton production accumulating as biomass (a negative ratio marks decreasing biomass). As illustrated in Figure 2c, the satellite-derived annual cycle in the r:μ ratio indicates a rapid increase in early winter, coincident with initiation of the blooming phase. By midwinter, >10% of phytoplankton production may be accumulating as biomass (Figure 2c, red line). The r:μ ratio then takes a downturn and decreases until the end of the bloom. These blooming-phase changes in r:μ are closely reproduced in timing and magnitude by the BEC-CCSM (Figure 2c, green line). Both approaches thus show that a smaller and smaller fraction of total phytoplankton production accumulates as biomass as spring stratification proceeds (data to the right of dashed green line in Figure 2c). It is this "recoupling" between phytoplankton division and losses that constrains r to its relatively narrow range during the blooming phase (Figure 2b), despite substantial springtime increases in μ (Figure 2a) (see additional discussion below).

[36] Further inspection of BEC-CCSM data shows that seasonal changes in phytoplankton losses (l) are dominated by mortality to zooplankton grazing (Figure 2d). This finding is consistent with a long history of modeling and field studies [e.g., *Evans and Parslow*, 1985; *Frost*, 1987; *Banse*, 1992, 2002; *Calbet and Landry*, 2004; *Landry and Calbet*, 2004; *Longhurst*, 2007; *Landry et al*., 2011].

[37] All ecosystem models are oversimplifications of natural systems. In the BEC-CCSM, for example, zooplankton

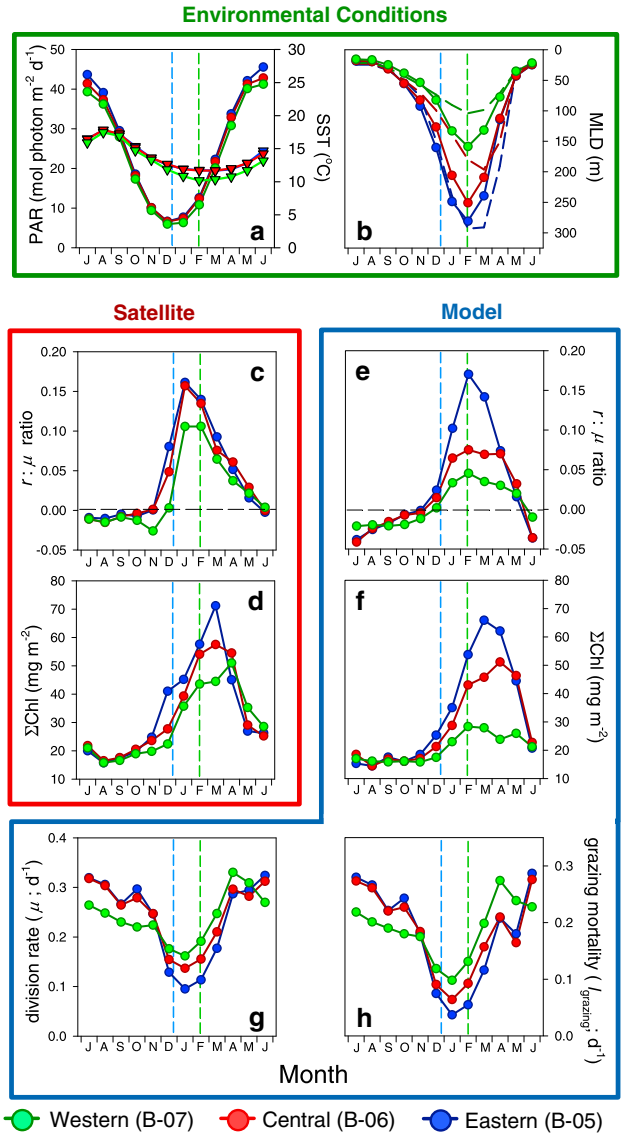

Figure 3. Longitudinal differences in subarctic Atlantic environmental and plankton properties for bins in the latitudinal zone of 45°N–50°N (Figure 1a). Easternmost bin (B-05; blue line), central bin (B-06; red line), and westernmost bin (B-07; green line). (a) Incident PAR (left axis; circles) and SST (right axis; inverted triangles). (b) Mixed layer depth (MLD) from data assimilating models (solid lines with circles; see section 2) and the BEC-CCSM (dashed lines). (c, d) Satellite-derived plankton properties (red box). (e–h) BEC-CCSM-based plankton properties (blue box). Ratio of phytoplankton specific net accumulation rate to division rate ($r:\mu$) and depth-integrated chlorophyll (ΣChl). Phytoplankton-specific division rate (μ). Grazing mortality rate ($l_{grazing}$). Data in all plots are monthly mean values for the period 1997–2007 and are plotted beginning in July on the left to focus on the autumn-through-spring period critical to bloom development. Dashed vertical light blue and green lines are same as in Figure 1b.

vertical migration is not accounted for, a single zooplankton population is assumed to graze on all phytoplankton groups, grazing rates are assumed independent of phytoplankton species composition, no account is made for zooplankton life histories (e.g., seasonal hibernation), and a very simplistic description is used for zooplankton predation by higher trophic levels. Nevertheless, the reasonable correspondence between satellite and BEC-CCSM rates shown in Figure 2 suggests that the model captures primary processes governing these annual cycles.

[38] One important relationship accounted for by the BEC-CCSM is that grazing losses are proportional to the product of predator-prey concentrations (i.e., $[C_{phyto}] \times [C_{zoo}]$) at low, nonsaturating prey abundances (see Table S1 in the supporting information). As a result, the specific rate of grazing on phytoplankton scales with the grazer concentration (i.e., $l_{grazing} \propto [C_{zoo}]$) and the specific division rate of the grazer population scales with phytoplankton concentration (i.e., $\mu_{zoo} \propto [C_{phyto}]$). In the model, the observed summer through autumn decreases in phytoplankton concentration (Figure 1b) result in a reduction in μ_{zoo}, declining $[C_{zoo}]$, and a concomitant decrease in $l_{grazing}$ (Figure 2d). This seasonal pattern in $l_{grazing}$ is modulated to a substantial degree by mixed layer deepening, which entrains relatively plankton-free water from below [*Evans and Parslow*, 1985; *Behrenfeld*, 2010]. This "dilution" effect of deep water entrainment does not directly impact the inventory (mg m^{-2}) of either phytoplankton or zooplankton, but it does decrease their concentrations (mg m^{-3}) and thus reduces both grazing efficiency and zooplankton growth. If the impacts of mixed layer deepening and decreasing temperature on $l_{grazing}$ are sufficiently large, then r may become positive under conditions that are simultaneously decreasing μ. Figures 2b and 2c show this transition to positive r occurring in early winter when MLD is rapidly deepening and growth conditions for phytoplankton are deteriorating. In short, the model suggests that initiation occurs because changes in environmental conditions from autumn into winter have a greater impact on zooplankton grazing than phytoplankton division rates, even though μ is decreasing rapidly.

3.3. Deeper Mixing and Lower Light Enhance Food Web Imbalances

[39] The relationship between mixed layer deepening and imbalances between μ and l can be further explored by comparing plankton properties between bins with differing winter mixing depths. For such an analysis, it is beneficial to compare data between bins from the same latitudinal zone. This approach better isolates the effects of dilution, since annual cycles of incident PAR and sea surface temperature (SST) are similar (Figure 3a). In the subarctic Atlantic, the depth of winter mixing decreases from east to west within a latitudinal band, as shown in Figure 3b for bins B-05, B-06, and B-07 (blue, red, and green lines, respectively). These three bins are the northernmost bins with satellite coverage for all months. Satellite and model data show that the between-bin differences in MLD yield an east-to-west decreasing pattern in winter and early spring $r:\mu$ (Figures 3c and 3e) and ΣChl (Figures 3d and 3f). In other words, deeper winter mixing causes larger imbalances between phytoplankton division and loss rates, such that a greater fraction of winter productivity accumulates as biomass in the east. However, deeper mixing also distributes the increasing phytoplankton population over a larger water volume, so initial

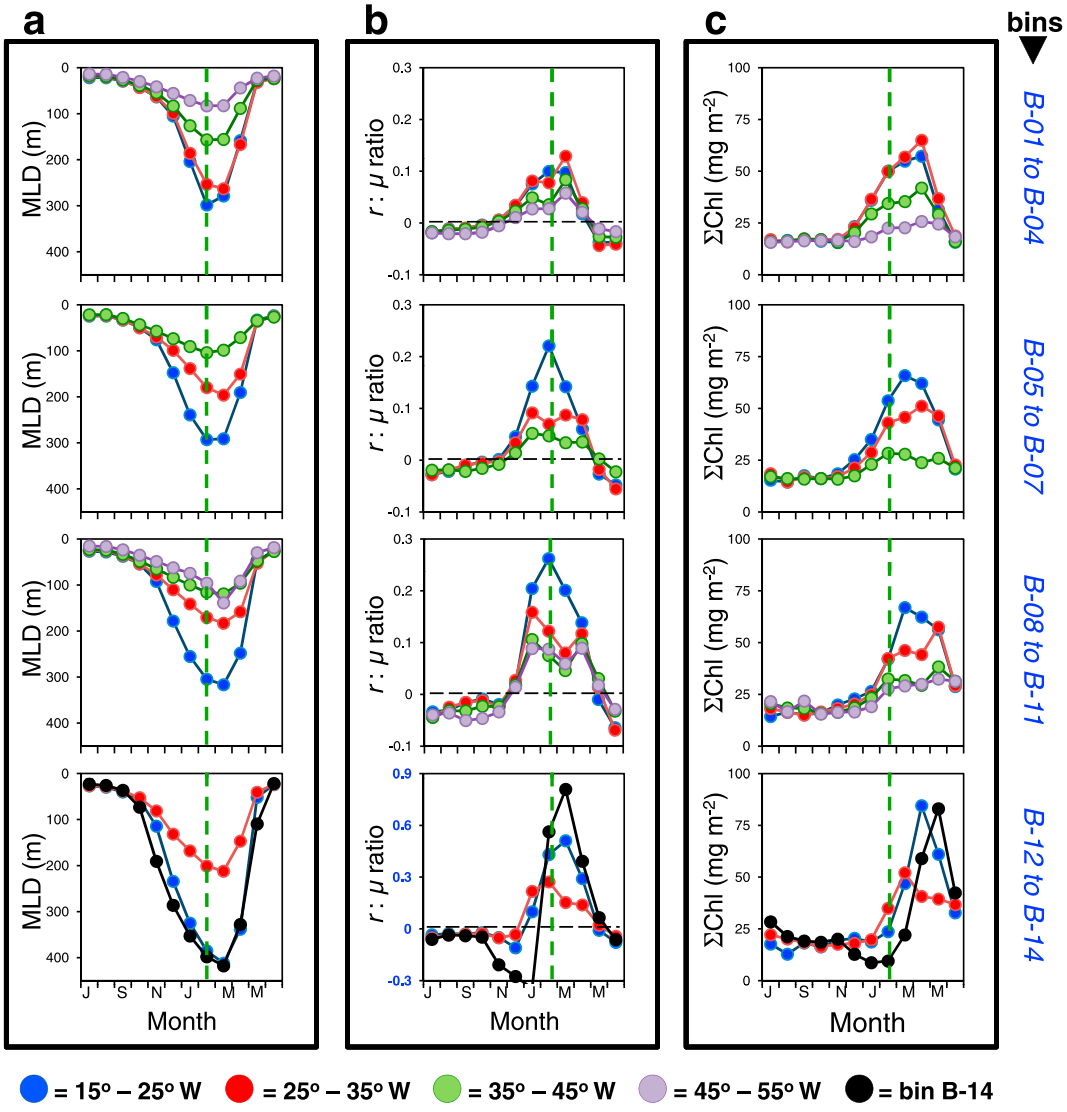

Figure 4. Key physical and ecosystems properties in all 14 subarctic Atlantic bins. (a) Mixed layer depth (MLD). (b) Ratio of net accumulation rate to division rate (r:μ). (c) Depth-integrated chlorophyll (ΣChl). Each row corresponds to a latitudinal set of bins from Figure 1a, increasing from south to north from the top of the figure to the bottom (bin numbers indicated in blue text on the right of each row). Colored circles and lines correspond to specific longitudinal zones, as defined at the bottom of figure. Black circles and lines correspond to bin B-14. The y axis ranges in each column are the same for all panels except the fourth panel of Figure 4b (emphasized by bold blue labels). Data in all plots are monthly mean values for the period 1997–2007 from the BEC-CCSM and are plotted beginning in July on the left to focus on the autumn-through-spring period critical to bloom development. Dashed vertical green line is same as in Figure 1b.

biomass accumulation is expressed as an increase in ΣChl (Figures 3d and 3f), rather than [Chl]. Another way of looking at this is that surface [Chl] fails to show the winter east-to-west increase expected from the purely physical effects of deeper (by hundreds of meters) mixing in the east because of the simultaneous and countering ecological impacts of mixing on phytoplankton-grazer interactions.

[40] The BEC-CCSM provides additional insights on the underlying ecology of the observed east-to-west patterns. Shallower mixing in the western bin (B-07) means that phytoplankton experience more sunlight each day during the winter and accordingly have higher specific division rates (μ) (Figure 3g, green line). In the east, winter μ values are lower because deeper mixing reduces daily light exposure (Figure 3g, blue and red lines). However, shallower mixing in the west also means that the dilution of phytoplankton and grazer populations is smaller, resulting in winter-through-spring grazing mortality that is proportionately higher (Figure 3h). This enhanced grazing counters the faster phytoplankton division rates in the west, giving a net result of lower peak values of ΣChl (Figure 3f).

[41] The depth of convective mixing varies not only from east to west but also from north to south (Figure 4a), along with daily light levels. Evaluation of

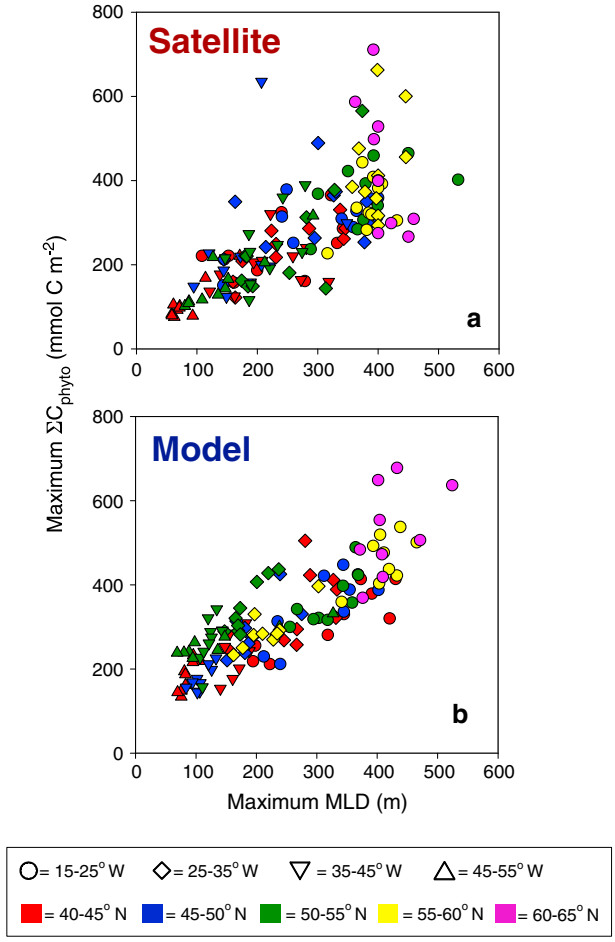

Figure 5. Relationship between maximum winter mixed layer depth (MLD) and maximum depth-integrated phytoplankton biomass (ΣC_{phyto}) for all bins and all years over the 1997–2007 period. (a) Satellite results ($R = 0.75$; $p < 0.001$; slope = 0.85 mmol C m^{-2} m^{-1}). (b) BEC-CCSM results ($R = 0.84$; $p < 0.001$; slope = 0.81 mmol C m^{-2} m^{-1}). Symbols and colors indicate bin longitudinal and latitudinal zone, respectively (see key at bottom of figure). For comparisons between maximum MLD and maximum ΣChl, see Figure S5, and between maximum MLD and bloom climax [Chl] and [C_{phyto}], see Figure S10.

basin-wide BEC-CCSM results indicates that deeper mixing and lower light consistently yield greater winter decoupling between phytoplankton division and grazing losses (i.e., r:μ ratio; Figure 4b) and, consequently, larger peak phytoplankton inventories (Figure 4c). Similar results are found for the satellite data (Figure S4 in the supporting information). Finally, winter mixing depth also varies from year to year. When annual maxima in MLD and ΣC_{phyto} are compiled for all regions and years, strong positive correlations are found between these two properties for both the satellite ($R = 0.75$) and model ($R = 0.84$) approaches (Figure 5). Similar positive correlations are also observed between MLD and ΣChl maxima (Figure S5 in the supporting information), despite this broad compilation of data encompassing a wide range in SST and PAR conditions (Figure S6 in the supporting information) that can potentially be associated with large changes in Chl:C_{phyto} ratios.

3.4. The Subarctic Atlantic "Disturbance and Recovery" Cycle

[42] Disruption of predator-prey relations by early winter mixing is only one phase in the annual subarctic Atlantic plankton cycle. The blooming phase continues through spring and, after its climax, is followed by a prolonged period of declining biomass (i.e., negative r) (Figures 2b, 3c, 3e, and 4b). Over this annual cycle, a variety of "bottom-up" factors can constrain phytoplankton division rates (μ). The relative importance of these different factors is largely inaccessible from remote sensing, but they are quantified in the BEC-CCSM. Figure 6 shows annual cycles in the severity of light, nitrogen, iron, phosphate, and silicate (diatoms only) limitation for the model "non-diatom" and "diatom" phytoplankton groups. Figure 6 corresponds to the 25°W to 35°W longitudinal band and is arranged top to bottom from 65°N to 40°N latitude (i.e., bins B-14, B-13, B-09, B-06, and B-02, respectively, as in Figure 1a). Also shown along the x axis of each panel is a black triangle identifying the onset of the winter-spring blooming phase. For all bins, nutrients are the dominant limiting factor for μ in the summer, transitioning to light limitation in autumn. In each case, bloom initiation occurs after significant relaxation of nutrient limitation and typically before maximum light limitation. In other words, timing of the initiation event does not correspond to any particular feature in the bottom-up factors regulating μ, particularly for the non-diatom group that dominates during the early phase of the bloom (Figure 6, left column). Nevertheless, bottom-up factors (especially light limitation) do play a role in modifying annual cycles of r.

[43] As described above, light-driven decreases in μ and dilution of the phytoplankton population by mixed layer deepening drive a decrease in zooplankton concentration in autumn. These impacts on the zooplankton community are sufficiently severe that eventually the decreases in $l_{grazing}$ cause $l < \mu$, at which point the phytoplankton population begins to increase. If this increase were to result in an increase in [C_{phyto}], the rise in food availability would stimulate a subsequent increase in zooplankton, thereby dampening any potential bloom. However, continued deepening of the mixed layer allows the increasing phytoplankton inventory (mg m^{-2}) to actually be associated with decreasing concentrations (mg m^{-3}), which accordingly further diminish (starve) the grazer population. This decoupling of μ and l continues at least until the annual maximum in MLD, at which point the r:μ ratio is at or near its annual maximum.

[44] Cessation of mixed layer deepening is a turning point in the blooming phase because the excess of μ over l, which has existed for well over a month, now results in an increase in [C_{phyto}]. In other words, positive r now increases both phytoplankton concentration and inventory. As resolved by the BEC-CCSM, the increase in [C_{phyto}] fuels an increase in grazer biomass and $l_{grazing}$ (e.g., Figure 3h). If we could hold μ constant for the remainder of spring, this grazing response to increasing phytoplankton concentration would rapidly decrease r (i.e., $\mu - g$ [C_{zoo}] would get smaller with time). However, concurrent springtime MLD shoaling and rising

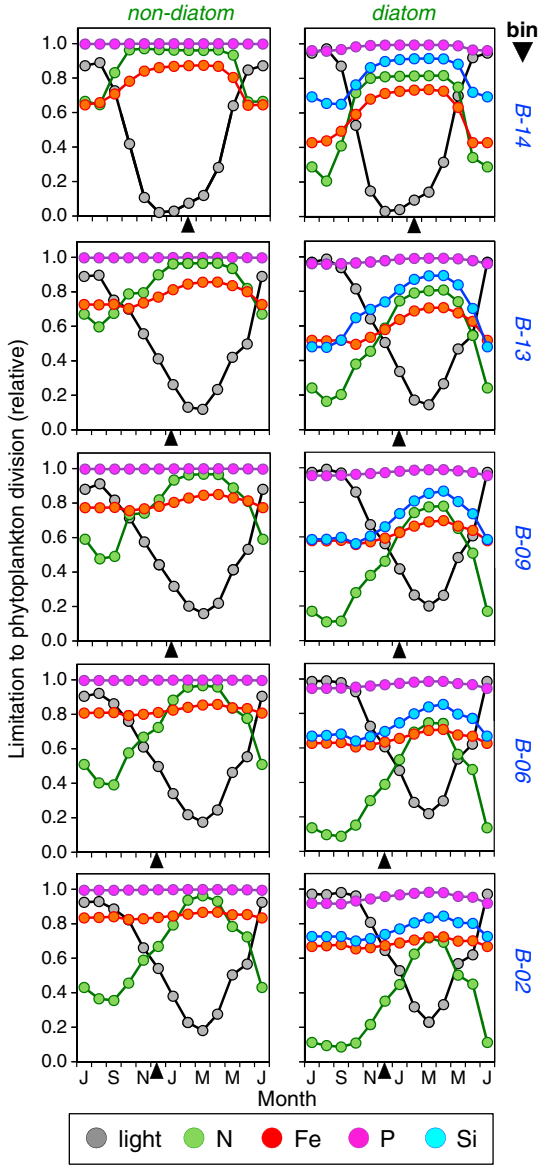

Figure 6. Relative importance of different environmental factors limiting phytoplankton division rates over the annual cycle. The (left) "non-diatom" and (right) "diatom" phytoplankton groups in the BEC-CCSM. Circles and line colors in each panel distinguish division-limiting factor (defined at bottom of figure). Severity of limitation (y axes) refers to achieved division rate relative to maximum potential division rate and thus ranges from 0 = complete limitation to 1 = no limitation. Panels in each column are for the 25°W to 35°W longitudinal band in Figure 1a and are arranged top-to-bottom from 65°N to 40°N latitude (bin numbers shown in blue text on the right). Black triangle along each x axis identifies onset of blooming phase. Data in all plots are monthly mean values for the period 1997–2007 and are plotted beginning in July on the left to focus on the autumn-through-spring period critical to bloom development.

PAR drive increases in μ that counter the growing losses to grazers, thereby perpetuating the bloom. Thus, the imbalance between l and μ initiated in early winter largely by physical processes (i.e., dilution) is sustained through spring by an interplay between concentration-driven increases in l and light-driven increases in μ. The magnitude of this imbalance is regulated in part by the relative rate of change in l and μ (Figures 3g and 3h), but not the absolute value of μ (e.g., compare Figures 2a and 2b). Thus, r may be just as large in February and March (low μ) as it is in May and June (maximum μ) (e.g., Figure 2b).

[45] The view that emerges from this description is a portrayal of the subarctic Atlantic bloom as an annually repeated "disturbance and recovery" cycle, where predator-prey interactions are disrupted by environmental forcings and subsequently recovered by ecosystem feedbacks. Bloom initiation represents an important tipping point in this cycle, marking where concurrent but unequal autumn-to-winter decreases in grazing and phytoplankton division first cause l to become smaller than μ. This threshold is crossed earliest in our southernmost bins, where the relatively elevated daily light flux allows μ to exceed l after only modest dilution impacts on $l_{grazing}$ (e.g., Figure 4b). With increasing latitude, light-driven decreases in μ are more substantial and thus require greater decreases in $l_{grazing}$ for bloom initiation (Figure 7). In other words, the autumn–early winter period of phytoplankton decline is longer at higher latitudes and bloom initiation is delayed, although still occurring prior to mixed layer shoaling. The more severe reduction in grazers with increasing latitude is reflected by the increasing r:μ ratios within a given longitudinal band (Figure 4b), and this greater impact on grazers contributes to the higher values of r in more northern bins during subsequent spring stratification (e.g., Figure 7). At extreme latitudes experiencing polar night, phytoplankton division ceases ($\mu = 0$ day^{-1}) and bloom initiation must await a rise in sunlight. During this period, zooplankton mortality continues and, when phytoplankton growth finally does commence, μ and l can be strongly decoupled. This condition is best illustrated by our bin B-14, where delayed bloom initiation and severe predator-prey decoupling (black symbols in Figure 4b, bottom) results in the strongest spring peak in r (Figure 7). Importantly, springtime values of μ for this bin do not exceed those for the lower latitude bins, thus re-emphasizing that the rate of increase in phytoplankton concentration (r) during stratification does not reflect the absolute value of μ but rather an interplay between winter predator-prey decoupling and the relative rate of springtime increases in l and μ.

3.5. Winter Losses and Springtime Detrainment

[46] Despite being oversimplifications of natural systems, contemporary ecosystem models are nevertheless complex and sensitive to choices of model parameters. A primary conclusion from the current study is that early-winter ecosystem processes play a critical role in the subarctic Atlantic bloom. During this period, two terms of importance in the BEC-CCSM are the temperature-dependent phytoplankton linear mortality rate ($\gamma(T)$, equation (6)) and the temperature-dependent maximum zooplankton growth rate ($Q10 = 2.0$; μ_{max} in Table S1 in the supporting information). To test the sensitivity of our results to these two key rates, we re-calculated annual cycles in r for μ_{max} with $Q10$ values ranging from 0 to 3.5 and with $\gamma(T)$ assigned a fixed value of either 0 day^{-1} or 0.1 day^{-1} (Figure S7 in the supporting information). These sensitivity runs show that modeled annual cycles of r are relatively unaffected either by the choice of $Q10$ value

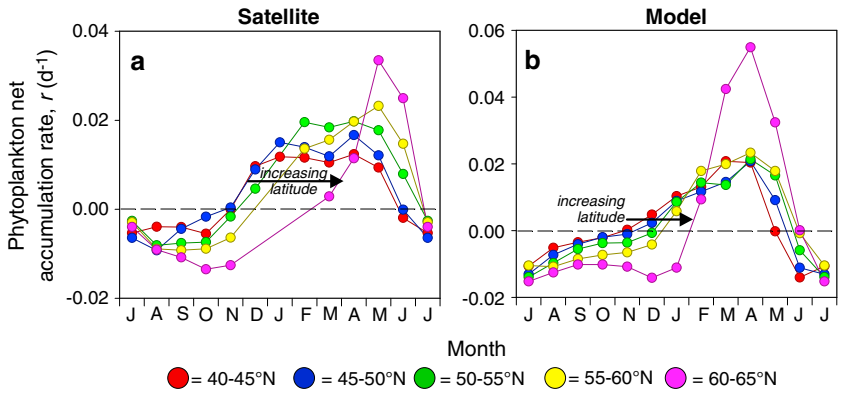

Figure 7. Latitudinal differences in annual cycles of phytoplankton net accumulation rates (r) for bins B-02, B-06, B-09, B-13, and B-14 (Figure 1a). (a) Satellite data. (b) BEC-CCSM data. Colors designate bin locations, as indicated at the bottom of the figure. Missing months in Figure 7a are due to lack of satellite coverage during the middle of winter at higher latitudes.

for μ_{max} or by assigning $\gamma(T)$ a value of 0 day^{-1}. Increasing $\gamma(T)$ to 0.1 day^{-1} reduces winter phytoplankton stocks, and thus zooplankton, and consequently prolongs the winter decline in biomass and yields a blooming phase that is delayed compared to observations. Future modeling efforts will benefit from additional field measurements that better constrain winter phytoplankton (and zooplankton) mortality rates.

[47] As detailed above in section 2.1, annual cycles in r reported here include an accounting for dilution effects during mixed layer deepening and a removal of detrainment effects during mixed layer shoaling. Only in this manner can the balance between phytoplankton division and loss rates within the mixed layer be accurately evaluated. *Behrenfeld* [2010, Figure 3] illustrated the error in retrieved values of r that can result from neglecting dilution effects, which cause changes in phytoplankton concentration to under-represent population net accumulation rates in autumn and winter. While mixed layer deepening spreads the active phytoplankton population over a growing volume of water, mixed layer shoaling in spring does not have the opposite effect of concentrating phytoplankton. Instead, phytoplankton deeper in the water column are detrained from the euphotic zone during spring shoaling and are subsequently lost through sinking or grazing. One consequence of detrainment is that it contributes to the late spring convergence of phytoplankton concentrations between bins (Figures 3d, 3f, and 4c). Specifically, MLDs across the subarctic basin shoal to similar depths during spring (e.g., Figures 3b and 4a), so a larger fraction of the wintertime phytoplankton inventory is lost (exported) to depth in areas of deeper winter mixing. With the BEC-CCSM, the significance of detrainment on total phytoplankton losses can be quantified by comparing annual cycles in r calculated using equations (3) and (4) with values calculated from phytoplankton inventories integrated to a fixed depth (e.g., annual maximum mixing depth; Figure S8 in the supporting information). This comparison shows that inclusion of detrainment losses decreases values of r during the spring and results in annual cycles that consistently peak prior to mixed layer shoaling (i.e., midwinter).

4. Discussion

[48] The critical depth hypothesis formalized by Sverdrup in 1953 encapsulated concepts introduced by *Gran and Braarud* [1935] and was consistent with earlier modeling studies [e.g., *Riley et al.*, 1949] in that it recognized changes in phytoplankton biomass as reflecting a balance between phytoplankton-specific division and loss rates. In Sverdrup's treatment, though, phytoplankton "respiration" per unit volume (which included all forms of phytoplankton losses) was assumed constant in time. This simplification had a major impact on the outcome of his analysis. Based on the choice of the "respiration" rate, a unique mixed layer light condition emerges where the light-dependent phytoplankton division rate equals the "respiration" rate. This specific point defines the "critical mixing depth," before which phytoplankton biomass must be decreasing and after which the rate of biomass increase is proportional to subsequent increases in μ. Certainly, Sverdrup understood that phytoplankton loss rates were not constant in time, but if loss rates are allowed to change in proportion to μ, then the concept of a critical depth loses its value because, even in the middle of winter, net biomass accumulation (positive r) becomes possible so long as μ is positive and losses have been sufficiently diminished. The study of *Behrenfeld* [2010] demonstrated that, indeed, r can be positive throughout the winter.

[49] Contemporary ocean ecosystem models, such as the BEC-CCSM, likewise build from the early work of *Riley et al.* [1949] but do not invoke a critical depth criterion. Instead, phytoplankton-specific division rates are linked to regulating environmental factors (e.g., temperature, nutrients, and light), zooplankton grazing is modulated by food availability, mortality, and often environmental properties (e.g., temperature), and attempts are made at mechanistically characterizing other phytoplankton loss processes (e.g., concentration-dependent aggregation leading to sinking). As illustrated here, this treatment yields strong positive correlations between μ and l, which is consistent with many earlier modeling and field-based studies [e.g., *Halldal*, 1953; *Steemann Nielsen*, 1958; *Pollingher and Berman*, 1977; *Tilzer*, 1984; *Evans and Parslow*, 1985; *Frost*, 1987;

Strom and Welschmeyer, 1991; *Banse*, 2002; *Longhurst*, 2007; *Calbet and Landry*, 2004; *Landry et al*., 2011]. Covariation of μ and l has a potential to largely divorce variations in r from variability in μ. This independence of r from μ was an important theme in the study of *Evans and Parslow* [1985], where development of phytoplankton blooms was viewed as a consequence of slight modifications in predator-prey interactions unfolding over the annual cycle.

[50] In *Behrenfeld* [2010], the transition from negative to positive r in early winter (while μ was still decreasing) was attributed to a disruption of predator-prey interactions by the dilution effects of mixed layer deepening. An equivalent effect was invoked in the studies of *Evans and Parslow* [1985] and *Marra and Barber* [2005]. Here we more directly test the significance of the dilution effect by examining phytoplankton properties between bins with differing winter mixing depths. Our results indicate that this physical-ecological interaction plays a critical role in initiating the blooming phase and governing the extent of winter-early spring decoupling between μ and l (as indexed by the r:μ ratio; e.g., Figures 3 and 4). By examining variability between bins and years, we also find a strong correspondence between winter MLD maxima and peak values of ΣC_{phyto} and ΣChl (Figures 5 and S5 in the supporting information). This result has a potentially significant implication. Specifically, forward projections of the BEC-CCSM have indicated that maximum winter mixed layer depths will become shallower over the next 100 years [*Danabasoglu et al*., 2012; *Meehl et al*., 2012], with average rates of change of 0.3 to 2.3 m yr^{-1} when aggregated into our 14 regional bins (Figure S9 in the supporting information). Applying the relationships given in Figure 5 to these projected changes in maximum MLD yields an average decrease in peak ΣC_{phyto} of 108 mmol C m^{-2} by year 2100 (range for the 14 bins: 22–190 mmol C m^{-2}), which is equivalent to a 40% reduction from current values (range 10%–66%). This simple calculation assumes that the response of subarctic Atlantic ecosystems to changes in winter MLD maxima remains consistent with present-day relationships. Nevertheless, the assessed change is certainly intriguing and warrants further analyses. It should also be noted that while we observe strong correlations between maximum MLD and phytoplankton inventories, similar correlations are not found with climax phytoplankton concentrations (Figure S10 in the supporting information). This lack of correlation is in part due to the equalizing effects of detrainment discussed in section 3.5, but also reflects the fact that the bloom climax occurs many months after the winter MLD maximum and thus is influenced by winter mixed layer nutrient loading, nutrient losses (export) during the prolonged stratification period, the balance between phytoplankton division rate and grazing rate, species succession (phytoplankton and zooplankton), and many other factors. Simulating this complexity remains a major challenge for ecosystem modeling and an important direction for model refinement.

[51] Recorded changes in phytoplankton stocks allow net population accumulation rates, r, to be one of the only pelagic ecosystem rate terms directly detected from space. Integrating over sufficient spatial scales minimizes uncertainties in r associated with advection. Furthermore, uncertainties in satellite-retrieved stocks (e.g., chlorophyll, phytoplankton carbon) should have minimal impacts on r estimates because the variability in optically active constituents (e.g., pigments, colored dissolved organic matter) underlying stock algorithm errors [*Siegel et al*., 2005a, 2005b] is likely small during any 8 day period used in assessing r. Satellite r data, along with stock and μ estimates, thus provide valuable observations for evaluating model output. Ecosystem models, in turn, provide important insights on underlying mechanisms for observed change. Nevertheless, these two data sources used in the current study fail to resolve many ecological complexities. For example, many large grazers hibernate at depth during winter [*Longhurst and Williams*, 1979; *Miller*, 2004; *Longhurst*, 2007] and zooplankton metabolism may be more sensitive to low temperatures than phytoplankton division rates [*Rose and Caron*, 2007; *López-Urrutia*, 2008; *Taucher and Oschlies*, 2011]. During restratification, we show that grazer responses to increasing phytoplankton abundance are important to the recoupling of l and μ, but major changes in species composition are also occurring during this period. Indeed, the bloom in phytoplankton is not simply an accumulation of a few species, but rather encompasses a continuous succession of different species emerging briefly as dominant before residing again to the diverse background of secondary species [*Sosik et al*., 2010]. Larger zooplankton also re-emerge as significant components of the grazer population during spring restratification [*Longhurst and Williams*, 1979; *Miller*, 2004; *Longhurst*, 2007]. Additional studies are therefore needed to further evaluate the relative importance of these and many other processes occurring during the blooming phase and to better understand mechanisms governing the dynamic taxonomic variability of marine ecosystems [*Giovannoni and Vergin*, 2012].

[52] Since the early work of *Gran and Braarud* [1935], *Riley et al*. [1949], and *Sverdrup* [1953], interpretations of phytoplankton blooms have been continuously revised and refined. The *Behrenfeld* [2010] study re-invigorated the debate on factors controlling bloom initiation by using satellite data to de-emphasize bottom-up factors and refocus attention on physical processes disrupting predator-prey interactions. Subsequent publications by *Chiswell* [2011], *Taylor and Ferrari* [2011], and *Mahadevan et al*. [2012] have argued again in favor of more traditional light-driven explanations for bloom initiation, but these studies do not address many of the issues raised by the earlier investigation. Here we capitalize on basin-wide differences in light and MLD conditions to further delineate the ecological underpinnings of annual plankton bloom cycles and their links to physical processes, while also noting a role for bottom-up factors in modulating these cycles. As in *Behrenfeld* [2010], our focus has once again been on the subarctic Atlantic, but our aim is to understand processes that transcend a single regional event and to build toward a more "general theory" of phytoplankton blooms. To this end, the recently coined "dilution-recoupling hypothesis" has here been restated and elaborated upon in the broader context of a "disturbance-recovery" process. In the subarctic Atlantic, deep winter mixing and low light provide the necessary ecosystem disturbance to yield a bloom. Different sources of disturbance can play an equivalent role in bloom initiation in other regions of the global ocean, such as monsoon forcing in the Arabian Sea [*Marra and Barber*, 2005], upwelling in coastal systems [*Cushing*, 1959], and iron deposition in high-nutrient, low-chlorophyll

waters [*Hamme et al*., 2010]. In each case, a disturbance "opens a window" for phytoplankton division to temporarily outpace losses, and in all cases, subsequent ecosystem feedbacks tighten predator-prey coupling again to reclose this window over the course of the bloom.

[53] **Acknowledgments.** We thank Robert O'Malley for compilation of satellite data and Kimberly H. Halsey and Allen J. Milligan for comments on the manuscript. This work was supported by the National Aeronautics and Space Administration, Ocean Biology and Biogeochemistry Program (grants NNX10AT70G, NNX09AK30G, NNX08AK70G, NNX07AL80G, and NNX08AP36A) and the Center for Microbial Oceanography Research and Education (C-MORE; grant EF-0424599), a National Science Foundation-supported Science and Technology Center.

References

Armstrong, R. A., C. Lee, J. I. Hedges, S. Honjo, and S. G. Wakeham (2002), A new, mechanistic model for organic carbon fluxes in the ocean based on the quantitative association of POC with ballast minerals, *Deep Sea Res. II*, *49*, 219–236.

Backhaus, J. O., E. Hegseth, H. Wehde, X. Irigoien, K. Hatten, and K. Logemann (2003), Convection and primary production in winter, *Mar. Ecol. Prog. Ser.*, *215*, 1–14.

Banse, K. (1992), Grazing, temporal changes of phytoplankton concentrations, and the microbial loop in the open sea, in *Primary Productivity and Biogeochemical Cycles in the Sea*, edited by P. G. Falkowski and A. D. Woodhead, pp. 409–440, Plenem, New York

Banse, K. (2002), Steeman Nielsen and the zooplankton, *Hydrobiologia*, *480*, 15–28.

Baudoux, A. C., A. A. M. Noordeloos, M. J. W. Veldhuis, and C. P. D. Brussaard (2006), Virally induced mortality of *Phaeocystis globosa* during two spring blooms in temperate coastal waters, *Aquat. Microb. Ecol.*, *44*, 207–217.

Behrenfeld, M. J. (2010), Abandoning Sverdrup's Critical Depth Hypothesis on phytoplankton blooms, *Ecology*, *91*(4), 977–989.

Behrenfeld, M. J., and P. G. Falkowski (1997), Photosynthetic rates derived from satellite-based chlorophyll concentration, *Limnol. Oceanogr.*, *42*, 1–20.

Behrenfeld, M. J., E. Boss, D. A. Siegel, and D. M. Shea (2005), Carbon-based ocean productivity and phytoplankton physiology from space, *Global Biogeochem. Cycles*, *19*, GB1006, doi:10.1029/2004GB002299.

Bidle, K. D., and A. Vardi (2011), A chemical arms race at sea mediates algal host-virus interactions, *Curr. Opin. Microbiol.*, *14*, 449–457.

Blain, S., et al. (2004), Availability of iron and major nutrients for phytoplankton in the northeast Atlantic Ocean, *Limnol. Oceanogr.*, *49*, 2095–104

Boss, E., and M. J. Behrenfeld (2010), In-situ evaluation of the initiation of the North Atlantic phytoplankton bloom, *Geophys. Res. Lett.*, *37*, L18603, doi:10.1029/2010GL044174.

Boss, E., et al. (2008), Observations of pigment and particle distributions in the western North Atlantic from an autonomous float and ocean color satellite, *Limnol. Oceanogr.*, *53*, 2112–2122.

Bratbak, G., J. K. Egge, and M. Heldal (1993), Viral mortality of the marine alga *Emiliania huxleyi* (Haptophyceae) and termination of algal blooms, *Mar. Ecol. Prog. Ser.*, *93*, 39–48.

Calbet, A., and M. R. Landry (2004), Phytoplankton growth, microzooplankton grazing, and carbon cycling in marine systems, *Limnol. Oceanogr.*, *49*, 51–57.

Campbell, J., et al. (2002), Comparison of algorithms for estimating primary productivity from surface chlorophyll, temperature and irradiance, *Global Biogeochem. Cycles*, *16*(3), 1035, doi:10.1029/2001GB001444.

Carr, M.-E., et al. (2006), A comparison of global estimates of marine primary production from ocean color, *Deep Sea Res.*, *53*, 741–770.

Chassot, E., et al. (2010), Global marine primary production constrains fisheries catches, *Ecol. Lett.*, *13*, 495–505.

Chiswell, S. M. (2011), Annual cycles and spring blooms in phytoplankton: Don't abandon Sverdrup completely, *Mar. Ecol. Prog. Ser.*, *443*, 39–50.

Clancy, R. M., and W. D. Sadler (1992), The Fleet Numerical Oceanography Center suite of oceanographic models and products, *Weather Forecasting*, *7*, 307–327.

Cushing, D. H. (1959), The seasonal variation in oceanic production as a problem in population dynamics, *J. Cons. Int. Explor. Mer*, *24*, 455–64.

Danabasoglu, G., et al. (2012), The CCSM4 ocean component, *J. Clim.*, *25*, 1361–1389.

D'Asaro, E. A. (2008), Convection and the seeding of the North Atlantic bloom, *J. Mar. Syst.*, *69*, 233–237.

Doney, S. C., S. Yeager, G. Danabasoglu, W. G. Large, and J. C. McWilliams (2007), Mechanisms governing interannual variability of upper ocean temperature in a global hindcast simulation, *J. Phys. Oceanogr.*, *37*, 1918–1938.

Doney, S. C., et al. (2009a), Skill metrics for confronting global upper ocean ecosystem-biogeochemistry models against field and remote sensing data, *J. Mar. Syst.*, *76*, 95–112, doi:10.1016/j.jmarsys.2008.05.015.

Doney, S. C., et al. (2009b), Mechanisms governing interannual variability in upper-ocean inorganic carbon system and air-sea CO_2 fluxes: Physical climate and atmospheric dust, *Deep Sea Res. II*, *56*, 640–655.

Ducklow, H. W., and R. P. Harris (1993), Introduction to the JGOFS North Atlantic Bloom Experiment, *Deep Sea Res. II*, *40*, 1–8.

Eppley, R. W. (1972), Temperature and phytoplankton growth in the sea, *Fishery Bull.*, *17*, 15–24.

Evans, G. T., and J. S. Parslow (1985), A model of annual plankton cycles, *Biol. Oceanogr.*, *3*, 327–347.

Frost, B. W. (1987), Grazing control of phytoplankton stock in the open subarctic Pacific Ocean: A model assessing the role of mesozooplankton, particularly the large calanoid copepodes *Neocalanus* spp., *Mar. Ecol. Prog. Ser.*, *39*, 49–68

Garver, S. A., and D. A. Siegel (1997), Inherent optical property inversion of ocean color spectra and its biogeochemical interpretation: I. Time series from the Sargasso Sea, *J. Geophys. Res.*, *102*, 18,607–18,625.

Geider, R. J., H. L. MacIntyre, and T. M. Kana (1998), A dynamic regulatory model of phytoplankton acclimation to light, nutrients, and temperature, *Limnol. Oceanogr.*, *43*, 679–694.

Gent, P. R., and J. C. McWilliams (1990), Isopycnal mixing in ocean circulation models, *J. Phys. Oceanogr.*, *20*, 150–155.

Gent, P. R., et al. (2011), The Community Climate System Model Version 4, *J. Clim.*, *24*, 4973–4991.

Giovannoni, S. J., and K. L. Vergin (2012), Seasonality in ocean microbial communities, *Science*, *335*, 671–6. doi:10.1126/science.1198078.

Gran, H. H., and T. Braarud (1935), A quantitative study on the phytoplankton of the Bay of Fundy and the Gulf of Maine including observations on hydrography, chemistry and morbidity, *J. Biol. Bd. Can.*, *1*, 219–467.

Halldal, P. (1953), Phytoplankton investigations from weather ship M in the Norwegian Sea, 1948–49, *Hvalråd. Skr.*, *38*, 1–91.

Hamme, R. C., et al. (2010), Volcanic ash fuels anomalous plankton bloom in subarctic northeast Pacific, *Geophys. Res. Lett.*, *37*, L19604, doi:10.1029/2010GL044629.

Key, R. M., et al. (2004), A global ocean carbon climatology: Results from Global Data Analysis Project (GLODAP), *Global Biogeochem. Cycles*, *18*, GB4031, doi:10.1029/2004GB002247.

Kistler, R., et al. (2001), The NCEP-NCAR 50-Year Reanalysis: Monthly means CD-ROM and documentation, *Bull. Am. Meteorol. Soc.*, *82*, 247–267.

Landry, M. R., and A. Calbet (2004), Microzooplankton production in the oceans, *ICES J. Mar. Sci.*, *61*, 501–507.

Landry, M. R., et al. (2011), Phytoplankton growth, grazing and production balances in the HNLC equatorial Pacific, *Deep-Sea Res. II*, *58*, 524–535.

Large, W. G., and S. G. Yeager (2009), The global climatology of an interannually varying air-sea flux data set, *Clim. Dyn.*, *33*, 341–364, doi:10.1007/s00382-008-0441-3.

Large, W. G., J. C. McWilliams, and S. C. Doney (1994), Oceanic vertical mixing: a review and a model with a nonlocal boundary layer parameterization, *Rev. Geophys.*, *32*, 363–403.

Lima, I., and S. C. Doney (2004), A three-dimensional, multi-nutrient, size-structured ecosystem model for the North Atlantic, *Global Biogeochem. Cycles*, *18*, GB3019, doi:10.1029/2003GB002146.

Longhurst, A. (2007), *Ecological Geography of the Sea*, Academic Press, San Diego, California.

Longhurst, A., and R. Williams (1979), Materials for plankton modelling: Vertical distribution of Atlantic zooplankton in summer, *J. Plankton Res.*, *1*, 1–29.

López-Urrutia, Á. (2008), The metabolic theory of ecology and algal bloom formation, *Limnol. Oceanogr.*, *53*, 2046–2047

Luo, C., N. Mahowald, and J. D. Corral (2003), Sensitivity study of meteorological parameters on mineral aerosol mobilization, transport and distribution, *J. Geophys. Res.*, *108*(D15), 4447, doi:10.1029/2003JD0003483.

Mahadevan, A., E. D'Asaro, C. Lee, and M. J. Perry (2012) Eddy-driven stratification initiates north Atlantic spring phytoplankton blooms, *Science*, *337*, 54–58.

Mahowald, N., C. Luo, J. D. Corral, and C. Zender (2003), Interannual variability in atmospheric mineral aerosols from a 22-year model simulation and observational data, *J. Geophys. Res.*, *108*(D12), 4352, doi:10.1029/2002JD002821.

Maritorena, S., D. A. Siegel, and A. R. Peterson (2002), Optimization of a semianalytical ocean color model for global-scale applications, *Appl. Opt.*, *41*, 2705–2714.

Marra, J., and R. T. Barber (2005), Primary productivity in the Arabian Sea: A synthesis of JGOFS data, *Prog. Oceanogr.*, *65*, 159–175.

McClain, C. R. (2009), A decade of satellite ocean color observations, *Annu.. Rev. Mar. Sci.*, *1*, 19–42.

Meehl, G. A., et al. (2012), Climate system response to external forcings and climate change projections in CCSM4, *J. Clim.*, *25*, 3661–3683.

Mémery, L., G. Reverdin, J. Paillet, and A. Oschlies (2005), Introduction to the POMME special section: Thermocline ventilation and biogeochemical tracer distribution in the northeast Atlantic Ocean and impact of mesoscale dynamics, *J. Geophys. Res.*, *110*, C07S01, doi:10.1029/2005JC002976.

Miller, C. B. (2004), *Biological Oceanography*, Blackwell, Oxford, United Kingdom, 402 pp.

Moore, C. M., et al. (2006a), Phytoplankton photoacclimation and photoadaptation in response to environmental gradients in a shelf sea, *Limnol. Oceanogr.*, *51*, 936–49

Moore, J. K., and O. Braucher (2008), Sedimentary and mineral dust sources of dissolved iron to the world ocean, *Biogeosciences*, *5*, 631–656.

Moore, J. K., and S. C. Doney (2007), Iron availability limits the ocean nitrogen inventory stabilizing feedbacks between marine denitrification and nitrogen fixation, *Global Biogeochem. Cycles*, *21*, GB2001, doi:10.1029/2006GB002762.

Moore, J. K., S. C. Doney, J. A. Kleypas, D. M. Glover, and I. Y. Fung (2002), An intermediate complexity marine ecosystem model for the global domain, *Deep Sea Res. II*, *49*, 403–462.

Moore, J. K., S. C. Doney, and K. Lindsay (2004), Upper ocean ecosystem dynamics and iron cycling in a global 3-D model, *Global Biogeochem. Cycles*, *18*, GB4028, doi:10.1029/2004GB002220.

Moore, J. K., S. C. Doney, K. Lindsay, N. Mahowald, and A. F. Michaels (2006b), Nitrogen fixation amplifies the ocean biogeochemical response to decadal timescale variations in mineral dust deposition, *Tellus, Ser. B*, *58*, 560–572.

Morel, A. (1991), Light and marine photosynthesis: A spectral model with geochemical and climatological implications, *Prog. Oceanogr.*, *26*, 263–306.

Morel, A., and J.-F. Berthon (1989), Surface pigments, algal biomass profiles, and potential production of the euphotic layer: Relationships reinvestigated in view of remote-sensing applications, *Limnol. Oceanogr.*, *34*, 1,545–1,562.

Moss, R. H., et al. (2010), The next generation of scenarios for climate change research and assessment, *Nature*, *463*, 747–756

Najjar, R. G., et al. (2007), Impact of circulation on export production, dissolved organic matter and dissolved oxygen in the ocean: Results from Phase II of the Ocean Carbon-Cycle Model Intercomparison Project (OCMIP-2), *Global Biogeochem. Cycles*, *21*, GB3007, doi:10.1029/2006GB002857.

Nielsdottir, M. C., C. M. Moore, R. Sanders, D. J. Hinz, and E. P. Achterberg (2009), Iron limitation of the postbloom phytoplankton communities in the Iceland Basin, *Global Biogeochem. Cycles*, *23*, GB3001, doi:10.1029/2008GB003410 .

Pollingher, U., and T. Berman (1977), Quantitative and qualitative changes in the phytoplankton of Lake Kinneret, Israel, 1972–1975, *Oikos*, *29*, 418–428.

Riley, G. A., H. Stommel, and D. F. Bumpus (1949), Quantitative ecology of the plankton of the western North Atlantic, *Bull. Bingham Oceanogr. Collect. Yale Univ.*, *12*, 1–169.

Rose, J. M., and D. A. Caron (2007), Does low temperature constrain the growth rates of heterotrophic protists? Evidence and implications for algal blooms in cold waters, *Limnol. Oceanogr.*, *52*, 886–895

Siegel, D. A., S. C. Doney, and J. A. Yoder (2002), The spring bloom of phytoplankton in the North Atlantic Ocean and Sverdrup's critical depth hypothesis, *Science*, *296*, 730–733.

Siegel, D. A., S. Maritorena, N. B. Nelson, M. J. Behrenfeld, and C. R. McClain (2005a), Colored dissolved organic matter and its influence on the satellite-based characterization of the ocean biosphere, *Geophys. Res. Lett.*, *32*, L20605, doi:10.1029/2005GL024310.

Siegel, D. A., S. Maritorena, N. B. Nelson, and M. J. Behrenfeld (2005b), Independence and interdependences among global ocean color properties: Reassessing the bio-optical assumption, *J. Geophys. Res.*, *110*, C07011, doi:10.1029/2004JC002527.

Sosik, H. M., J. J. Olson, and E. V. Armbrust (2010), Flow cytometry in phytoplankton research, in *Chlorophyll a Fluorescence in Aquatic Sciences: Methods and Applications, Dev. in Appl. Phycol.*, vol. *4*, edited by D. J. Suggett et al., Springer, Netherlands, doi:10.1007/978-90-481-9268-7_8.

Steemann Nielsen, E. (1958), The balance between phytoplankton and zooplankton in the sea, *J. Cons. Int. Explor. Mer.*, *23*, 178–188.

Strom, S. L., and N. A. Welschmeyer (1991), Pigment-specific rates of phytoplankton growth and microzooplankton grazing in the open subarctic Pacific, *Limnol. Oceanogr.*, *36*, 50–63.

Suttle, C. A., A. M. Chan, and M. T. Cottrell (1990), Infection of phytoplankton by viruses and reduction of primary productivity, *Nature*, *347*, 467–469.

Sverdrup, H. U. (1953), On conditions for the vernal blooming of phytoplankton, *J. Cons. Perm. Int. Explor. Mer.*, *18*, 287–295.

Takahashi, T., et al. (2009), Climatological mean and decadal change in surface ocean pCO_2 and net sea–air CO_2 flux over the global oceans, *Deep Sea Res. II*, *56*, 554–577.

Taucher, J., and A. Oschlies (2011), Can we predict the direction of marine primary production change under global warming?, *Geophys. Res. Lett.*, *38*, L02603, doi:10.1029/2010GL045934.

Taylor, J. R., and R. Ferrari (2011), Shutdown of turbulent convection as a new criterion for the onset of spring phytoplankton blooms, *Limnol. Oceanogr.*, *56*, 2293–2307, doi:10.4319/lo.2011.56.6.2293.

Tilzer, M. M. (1984), Estimation of phytoplankton loss rates from daily photosynthetic rates and observed biomass changes in Lake Constance, *J. Plankton Res.*, *6*, 309–324.

Townsend, D. W., M. D. Keller, M. E. Sieracki, and S. G. Ackleson (1992), Spring phytoplankton blooms in the absence of vertical water column stratification, *Nature*, *360*, 59–62.

Vardi, A., et al. (2009), Viral glycosphingolipids induce lytic infection and cell death in marine phytoplankton, *Science*, *326*, 861–865.

Wanninkhof, R. (1992), Relationship between wind speed and gas exchange over the ocean, *J. Geophys. Res.*, *97*, 7373–7382.

Ward, B. A., and J. J. Waniek (2007), Phytoplankton growth conditions during autumn and winter in the Irminger Sea, North Atlantic, *Mar. Ecol. Prog. Ser.*, *334*, 47–61.

Westberry, T. K., M. J. Behrenfeld, D. A. Siegel, and E. Boss (2008), Carbon-based primary productivity modeling with vertically resolved photoacclimation, *Global Biogeochem. Cycles*, *22*, GB2024, doi:10.1029/2007GB003078.

Yeager, S. G., C. A. Shields, W. G. Large, and J. J. Hack (2006), The low-resolution CCSM3, *J. Clim.*, *19*, 2545–2566.